

CANISIUS The Austrian Neutron Spin Echo Interferometer

Niels Geerits^{1,*}, Simon Hack¹, Ad van Well², Steven R. Parnell³, Hartmut Abele¹, and Stephan Sponar^{1†}

¹*Atominstytut, Technische Universität Wien, Stadionallee 2, 1020 Vienna, Austria*

²*Faculty of Applied Sciences, Delft University of Technology, Mekelweg 15, Delft 2629JB, The Netherlands*

³*ISIS, Rutherford Appleton Laboratory, Chilton, Oxfordshire, OX11 0QX, UK*

(Dated: August 13, 2024)

The broad band resonant spin echo interferometer, CANISIUS, is presented. CANISIUS is built in a versatile way, such that it can be operated in both a continuous broad band beam or a pulsed Time of Flight beam. This versatility also extends to the modes available to the instrument, such as Neutron Resonant Spin Echo, Spin Echo (Modulated) Small Angle Neutron Scattering and coherent averaging to produce structured wavefunctions for scattering. The instrument may also be used as an interferometer, to probe fundamental questions in quantum mechanics. In this paper we detail both the continuous and Time of Flight options of the instruments. In addition we demonstrate the applicability of our interferometer to ultra small angle scattering in a white beam. Finally we demonstrate a new spin echo interferometry tool, which uses incomplete recombination of the two path states to generate composite wavefunctions with special structure. In particular we show that this method produces neutron wavefunctions that exist in a superposition of two quantum mechanical OAM modes, $\ell = \pm 1$. We illustrate that just as this method can be used to generate certain structured waves, it may also be used to characterize the structure of the input wavefunction.

INTRODUCTION

Neutron interferometry is a powerful and established tool for addressing a variety of scientific challenges from exploring quantum state entanglement in massive particles [1, 2] and inertial effects on quantum particles such as gravitationally induced interference (COW experiment) [3], the Sagnac effect [4, 5] and the Mashhoon effect [6, 7], to nuclear physics questions by measuring scattering cross sections to high precision [8]. Furthermore interferometers may be used to create complex structured waves by coherent averaging [9, 10]. This method is particularly useful for producing vortex neutrons [10, 11], which carry Orbital Angular Momentum (OAM) and may have unique scattering properties [12–14]. Furthermore, OAM represents an additional quantum mechanical degree of freedom, which is useful for quantum information and contextuality experiments.

The most well known type of neutron interferometer is made from a perfect silicon crystal in triple Laue configuration [15], however other methods have been established as well such as supermirror based approaches [16] and magnetic refraction based approaches [17]. Neutron spin echo [18] techniques which use the latter method have been particularly successful. The classic spin echo technique, resonant spin echo [19] and "Modulation of Intensity Emerging from Zero Effort" (MIEZE) [20] interfere the two neutron spin states in time, which makes these techniques particularly sensitive to dynamic effects, such as those observed in inelastic scattering. In addition MIEZE has even been applied to observe violations of Bell's inequality [21, 22]. In 1996 Rekveldt proposed to apply spin echo small angle scattering (SESANS), by inclining the magnetic field regions with respect to the direct beam [23]. This approach splits and later focuses the two spin states transversely, which makes

the instrument sensitive to structure along the refraction direction [17]. In recent years many of the famous neutron interferometry experiments, such as the COW experiment [24, 25] and tests of quantum entanglement [26, 27] have been carried out with spin-echo type interferometers. In addition these interferometers have a few advantages over perfect crystal interferometers, such as the ability to accept a large, broad band and wide divergence beam. As a result spin-echo interferometer have a higher usable flux. In addition this class of interferometer is not as sensitive to temperature variations and vibrations. The most obvious disadvantage is the microscopic path separation (10 nm to 10 μ m), consequently the paths can usually not be manipulated separately. Nonetheless, the area spanned by the two paths of a spin echo interferometer is similar to that of a single crystal interferometer. In addition it is simpler to produce structured wavefunctions by coherent averaging with spin echo interferometers, due to the possibility of a modular design, which allows for an arbitrary number of beam splitters and paths in a single instrument.

In this paper we report on the new broad band spin-echo interferometer, CANISIUS (Coherent Averaging Neutron Instrument for Spin-echo Interferometry and fUndamental Science), designed to investigate the properties of vortex neutrons carrying non-zero OAM. CANISIUS follows similar design doctrines as the Offspec [28] and Larmor [29, 30] instruments at the ISIS neutron source. That is to say, CANISIUS uses adiabatic RF flippers [31] to ensure broad band efficiency, and is built in a modular way so that it can be applied to a variety of different modes (SESANS, SEMSANS [32], NRSE and MIEZE). In addition CANISIUS can quickly change between a continuous white beam and a pulsed beam for time of flight. Here we will report on the design and efficiency of the adiabatic RF-flippers and the instrument, the inter-

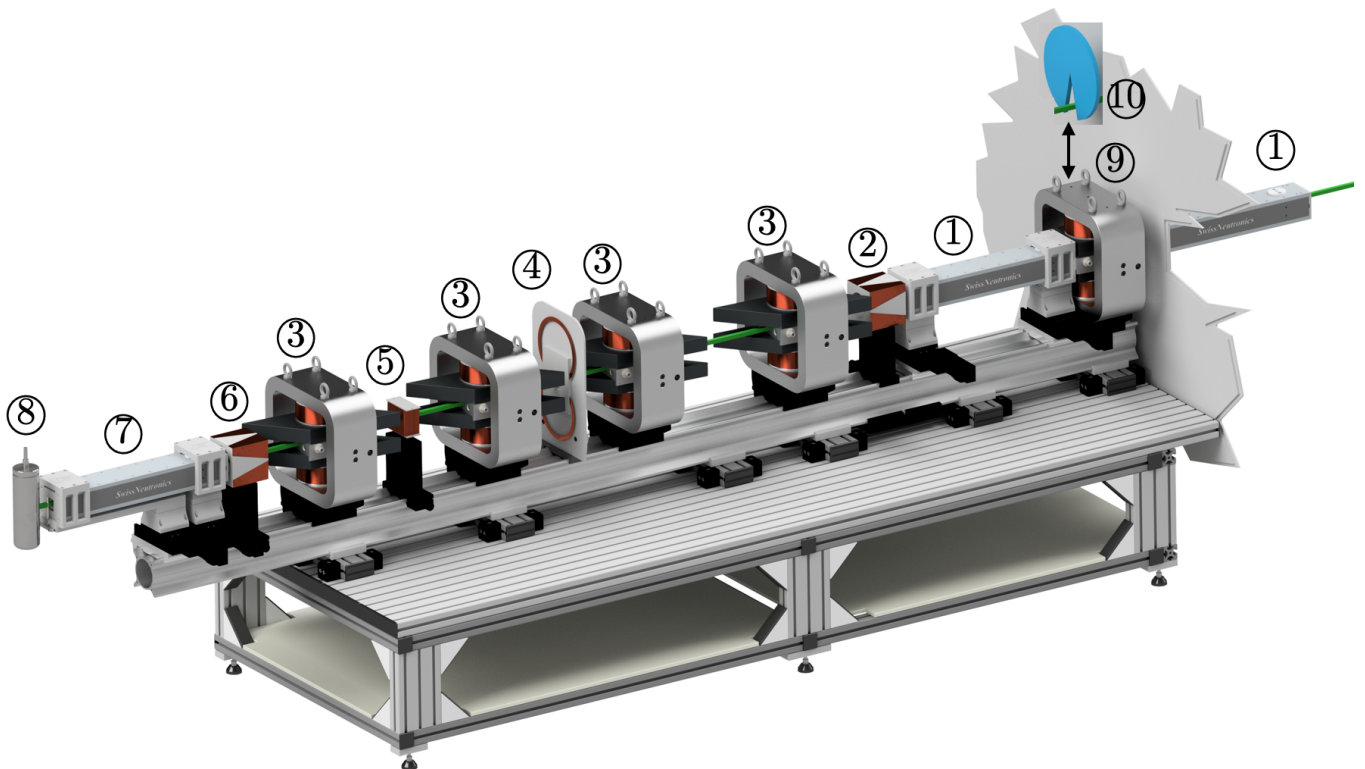


FIG. 1. Render of the CANISIUS instrument configured for white beam SESANS. The beam propagates from right to left. First the beam is polarised by double reflection from two single substrate $m=4$ polarising supermirrors (1). Next the polarisation is adiabatically rotated by 90 degrees by a v-coil (2). The beam then passes through a pair (arm 1) of adiabatic RF flippers with parallelogram shaped poleshoes, which act as the first beam splitter and mirror (3). A field stepper is positioned between the first and second pair (arm 2) of RF flippers, to facilitate a fast non-adiabatic field transition from arm 1 to arm 2 (4). Samples of various types may be inserted right before the field stepper. The second arm of RF flippers serve effectively as a mirror and beam splitter to recombine the split beams. Between the last two RF flippers the beam is passed through a precession coil (5). Finally before the spin is selected by the last polarising supermirror (7) the neutrons pass through a final v-coil facilitating another adiabatic 90 degree rotation (6). Neutrons passing the polarising supermirror are detected by a high-efficiency ^3He counting tube. In addition to the usual continuous mode of operation the CANISIUS instrument can also be operated in ToF mode. For this purpose two chopper device are available: a conventional mechanical chopper (10) as well as a spin-chopper system (9), consisting of an RF flipper in combination with the pre-polarizer, that is the very first supermirrors (1). The length of the instrument, given by the distance between chopper (9,10) and detector (8) is 3 meters.

ferograms produced by the instrument in broad-band and time of flight (ToF) SESANS modes and finally discuss production and investigation of vortex neutrons.

METHODS

Instrument Overview

A three dimensional render of the CANISIUS instrument in a SESANS configuration is shown in figure 1. CANISIUS is situated at the white beamline of the Atominstut (TU Wien) 250 kW reactor. The instrument can be operated in either a continuous broad-band or two distinct ToF modes. A standard mechanical chopper is used for the regular ToF mode. The second mode is en-

abled by a spin chopping system, which is made possible since the beam is initially polarized by double reflection from a pair of $m=4$ single flat substrate supermirrors, this allows the beam to be chopped by inserting a broad-band spin flipper between the two mirrors which can be pulsed [33, 34]. Due to the cut-off of the supermirrors the available wavelength range is $2\text{\AA} - 6\text{\AA}$, with a peak at 2.5\AA . After the double reflection polarizer the beam is passed through a v-coil which adiabatically rotates the neutron spin around the propagation axis from vertical to horizontal. In the first arm of the instrument which consists of a pair of adiabatic RF flippers [35], the two spin states are separated longitudinally (standard NRSE) and if parallelogram shaped poleshoes are employed also transversely (SESANS). The second arm with equal but opposite field of the first arm recombines the spin states.

Spatial overlap between the two spin states is ultimately measured by a spin projective measurement, which in practice is enabled by a v-coil and a supermirror. An additional closed coil in arm 2, allows variation of the phase between the two spin states. Finally a series of wedges can be inserted to change and calibrate the angle of the poleshoes by up to ± 5 degrees. This gives some more flexibility to tune the transverse spin state separation, however its primary purpose is to enable the new coherent averaging mode, to produce structured neutron waves. If both arms of the interferometer are operated at a different poleshoe angle the instrument fails to focus the spin states transversely. As a result some residual separation is left between the spin states. As we will show in a later section, this residual separation induces a structured wave with OAM. The residual separation may also be scanned, thus allowing one to measure the correlation between the spin up and down wavefunctions, similar to what is described in [36]. On average over the entire wavelength band the polarisation of the instrument in the non-echo mode (RF system and v-coils turned off), in which there should be no spin precession, is 0.904. The RF coils are matched to the output impedance of the amplifiers for operation at 1.4 MHz, however the coils may also be operated in resonant mode (ToF or monochromatic), in which case they can be operated at any frequency between 10 kHz and 5 MHz, since the power requirements are low (1-2 W) and the amplifiers are equipped to handle up to 400 W of reflected power. In the following subsections the adiabatic RF flippers, SESANS, the ToF modes and the coherent averaging mode will be discussed in more detail.

Adiabatic RF Spin Flippers

In this subsection we provide a detailed overview of the design of CANISIUS' RF flipper system. An RF flipper is depicted in figure 2, for 3 different poleshoe configurations, square for NRSE and MIEZE, parallelogram for SESANS and SEMSANS and tilted parallelogram for coherent averaging. The poleshoes in addition to the magnetic cores were machined from soft iron and subsequently heat treated. The yokes were machined from construction steel. Coils of 400 windings each are situated around each magnetic core. The gap between the poleshoes is 30 mm, in which the RF system is situated (figure 2 (d)). This RF system consists of an aluminium housing containing an 80 mm long RF coil with a diameter of 20 mm and a gradient coil which has minimal winding density in the center and increases towards in the ends of the coil. The RF coil consists of 2 mm copper tubing (inner diameter 1.5 mm) wound on a PEEK bobbin and encased in kapton foil to prevent arcing. 250 ml/min of G12 coolant is pumped through the tubing, to facilitate heat transport, the coolant is

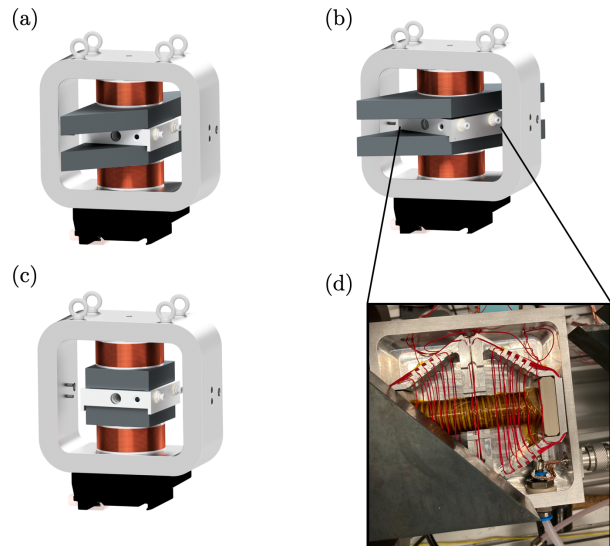


FIG. 2. Render of the adiabatic RF spin flippers with parallelogram shaped poleshoes at 45 deg (a), 45 ± 5 deg (b), and 90 deg in (c). The photo in (d) shows a top-view of one RF coil partly taken out of the parallelogram shaped poleshoes for demonstration purposes to see water the cooled RF coil, the gradient field coil, as well as the inlet of the coolant and the electrical conducting.

cooled to 3 degrees by a secondary loop connected to a chiller. Matching of the RF coils to the amplifier output is done capacitively for a single frequency, 1.4 MHz. Mica capacitors were used for their high stability and low loss at typical NRSE frequencies. In adiabatic flipping mode, roughly 60 W are dissipated in each coil, in addition to 40 W in each gradient coil. In resonant flipping mode only 1-2 W are required depending on the frequency, hence in this mode matching between load and amplifier is not necessary. The efficiency of a single adiabatic RF flipper is shown in figure 3, which is determined first by measuring the polarization in a non precessing mode (v-coil turned off) and then normalizing said polarization by the the instrument spin transport efficiency, which as mentioned earlier is 0.904. The polarization is calculated using the well known formula

$$P = \frac{I_+ - I_-}{I_+ + I_-} \quad (1)$$

with I_+ the intensity of the spin state aligned to the analyzing direction (i.e. when the flipper is turned on) and I_- the opposite spin state. Figure 3 demonstrates that our RF flippers have a constant flip efficiency over the entire wavelength band indicating a good adiabaticity of the flippers. A weighted average efficiency of 0.977 can be extracted from the data shown in figure 3. This is comparable to some other adiabatic RF flipper designs [37]. Though we note that flipping efficiency of 99% are possible with similar design [38]. In some other designs efficiencies of up to 99.9% have been reported [39].

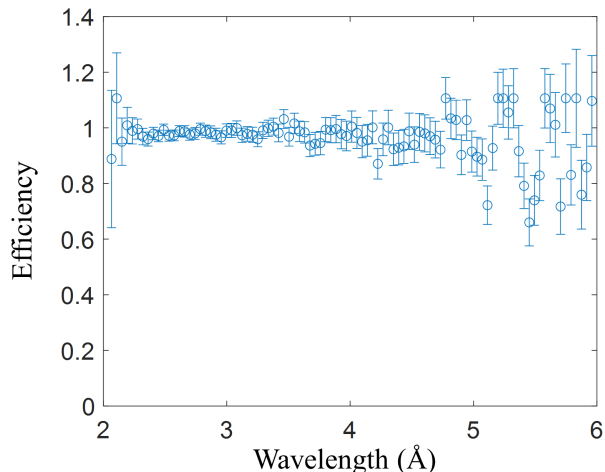


FIG. 3. Flipping efficiency of one adiabatic RF flipper against wavelength measured using the ToF technique. This is calculated using ToF spectrums with the flipper on and off, the result is finally normalised by the instrument efficiency of 0.904. The weighted average of the flipping efficiency over the entire spectrum is 0.977.

Time of Flight Options

CANISIUS has two options available for producing a pulsed beam. The first is a fermi like chopper which consists of stacked, short, straight, cadmium lined channels, which is spun at 50 Hz, resulting in an effective pulse frequency of 100 Hz. The second method, uses an RF flipper positioned between the two polarizing supermirrors. In this case the the two mirrors are oriented to select opposite spins, so that when the flipper is off no beam is transmitted into the instrument. In resonant mode the phase accumulated by a neutron in the flipper is given by

$$\alpha = \gamma B_{RF} t \quad (2)$$

with γ the gyromagnetic moment of the neutron B_{RF} the field strength and t the time for which the particle is exposed to the field. Hence if the RF pulse time is much shorter than the flight time through the device of the fastest neutron then this phase is wavelength independent. Therefore to produce a pulsed beam the RF flipper is simply shortly pulsed in resonant mode, which flips all neutrons that are in the RF coil at the time of the pulse. These neutrons can then be transmitted through the instrument and to the detector. This RF flipper is designed equivalently to the others described in the previous section, with the exception of the gradient coil, since this is not required. The RF field pulse length is $5 \mu s$, ten times shorter than the flight time of 2.5 \AA neutrons through the RF coil. This corresponds to 7 cycles of the RF field at 1.4 MHz. In figure 4 a comparison between the ToF spectra of the mechanical

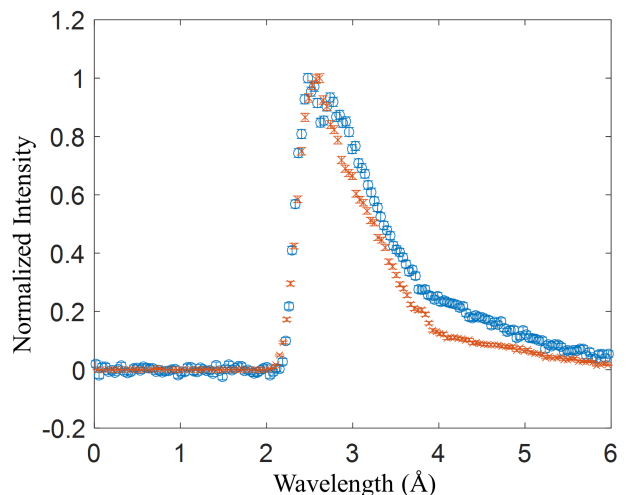


FIG. 4. Normalized Time of Flight spectra produced using the RF spin chopping device (blue circular data points) and the mechanical chopper (red cross shaped data points).

and spin chopper can be seen. It can be seen that for short wavelengths the chopper systems perform with equal relative efficiency, however at longer wavelengths the spin chopper has a higher transmission compared to the mechanical chopper. This is due to the wavelength dependent transmission of the mechanical fermi chopper [40] which we may approximate at long wavelengths by 1 minus the ratio between the channel width seen by a neutron of wavelength λ and the channel width when the chopper is at rest:

$$T = 1 - \frac{\omega m \lambda D^2}{4\pi d \hbar} \quad (3)$$

with ω the rotation frequency of the device, D the length and d the width of the channels. The transmission of the spin chopper on the other hand is independent of wavelength when the RF pulse time is much shorter than the flight time of the neutron through the RF coil. In this case, much like the double disk chopper [41], the wavelength resolution is also wavelength independent, depending only on the distance between the chopper and the detector, L and the length of the RF coil D

$$\frac{\Delta \lambda}{\lambda} = \frac{D}{L} \quad (4)$$

In addition the RF pulse frequency may be optimize the intensity for a given detector distance.

Spin Echo Small Angle Neutron Scattering

Spin Echo Small Angle Neutron Scattering (SESANS) is an interferometric spin echo technique first designed to resolve small angle scattering smaller than the beam

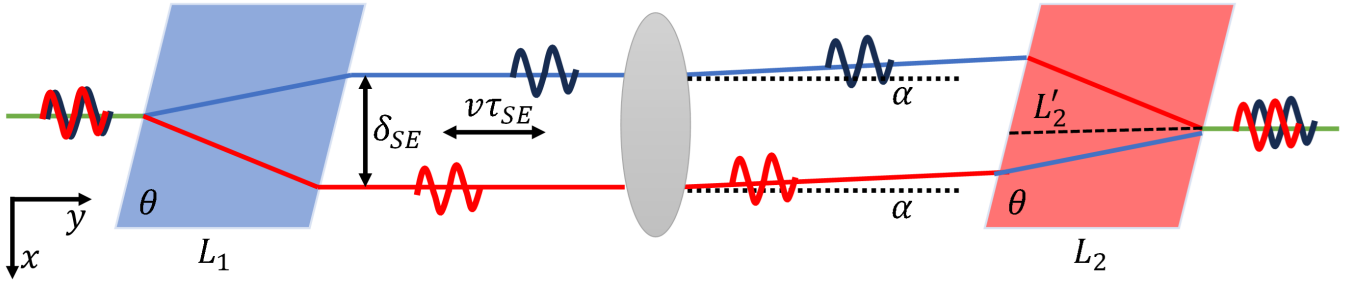


FIG. 5. Schematic representation of Spin Echo Small Angle Neutron Scattering. Two inclined magnetic field regions of opposite polarization (represented in light blue and red) are used to induce a transverse separation between the two neutron spin states, also indicated in blue and red. The SESANS configuration shown here also induces a longitudinal separation between the wavepackets indicated by $v\tau_{SE}$. The sample indicated in gray causes the beam to be scattered by a small angle α . As a result the path length through the second field region is changed L_2' , resulting in a net phase shift between the two spin states upon recombination.

divergence [23, 42]. Later the interferometric applications were further developed and applied to a variety of questions ranging from quantum contextuality [26, 27] to (exotic [25]) gravity [24] and to probe properties of the neutron itself, such as the intrinsic coherence of a single neutron [43]. Regular Spin Echo, uses two oppositely polarized field regions, such that all precession induced in the first field region is reversed in the second, if the neutron velocity does not change in the instrument, ie.

$$\gamma B_1 \frac{L_1}{v_1} = -\gamma B_2 \frac{L_2}{v_2} \quad (5)$$

with B the magnetic field strength, L the length of the precession region and v the neutron velocity. The index refers to the first or second precession region. It follows that such a spin echo instrument is sensitive to small changes of the neutrons kinetic energy. In SESANS the field regions are inclined (see figure 5), so that the instrument becomes sensitive to small changes in the neutrons transverse wavevector component, q (small angle scattering). If the velocity of the neutron is unchanged the net phase accumulated by the neutron after a small angle scattering event is simply

$$\chi = \gamma B_2 \frac{\Delta L_2}{v} \quad (6)$$

where ΔL_2 is the difference between the scattered and non-scattered neutron flight path length in the second arm, given by

$$\Delta L_2 = \cot(\theta_0)\alpha = \cot(\theta_0)\frac{q}{k} \quad (7)$$

with α the scattering angle. It follows that the phase is given by

$$\chi = \frac{\gamma m B_2 L_2 \cot(\theta_0) \lambda^2}{4\pi^2 \hbar} q = \delta_{SE} q \quad (8)$$

with the spin-echo length δ_{SE} equal to the induced transverse separation between the up and down spin

state. The polarisation is therefore a cosine transform of the scattering function $S(q)$

$$P = \int dq \cos(\delta_{SE}q) S(q) = G(\delta_{SE}) \quad (9)$$

with $G(\delta_{SE})$ the real space correlation function. Since δ_{SE} is proportional to λ , a white beam SESANS, such as CANISIUS, averages over many different correlation lengths.

$$P = \frac{\int d\lambda G(\delta_{SE}) I(\lambda)}{\int d\lambda I(\lambda)} \quad (10)$$

with $I(\lambda)$ the intensity distribution of the sampled beam. To extract the wavelength information an additional precession coil (see nr. 5 in figure 1), can be used to measure the spin echo group. This precession coil adds a phase which is field and wavelength dependent

$$\varphi = \frac{\gamma B m \lambda d}{2\pi \hbar} = \kappa \lambda \quad (11)$$

with d the length of the precession coil. Hence by adding the precession coil the polarisation becomes the cosine transform of the correlation function times the intensity distribution

$$P(\kappa) = \frac{\int d\lambda G(\delta_{SE}) I(\lambda) \cos(\kappa \lambda)}{\int d\lambda I(\lambda)} \quad (12)$$

It follows that the cosine transform of the polarisation of the spin echo group, $P(\kappa)$ yields the correlation function weighted by the normalized intensity distribution. The correlation function of a specific sample can be extracted by normalizing the cosine transform of the spin echo group with sample, $P_1(\kappa)$ by a cosine transform of the spin echo group without the sample, $P_0(\kappa)$.

$$G(\delta_{SE}) = \frac{\int d\kappa P_1(\kappa) \cos(\kappa \lambda)}{\int d\kappa P_0(\kappa) \cos(\kappa \lambda)} \quad (13)$$

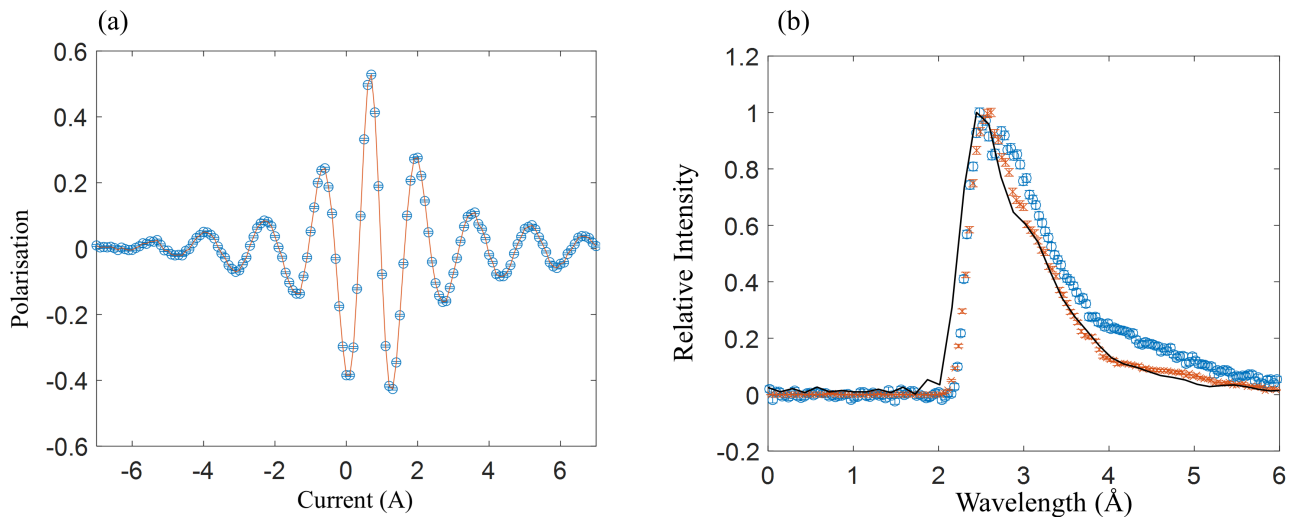


FIG. 6. (a) Polarisation of the spin echo group measured against current in the precession coil. The individual data points with errorbars are shown in blue and in interpolation of the data is shown in red. (b) The Fourier transform of the spin echo group is shown in black, while the spectra measured using both chopping techniques also shown in figure 4 is superposed.

Since the correlation function of a vacuum is constant, the cosine transform of the spin echo group without a sample should simply be equal to the normalized spectrum. In figure 6 one can see the spin echo group measured by CANISIUS and its Fourier transform superposed on the normalized ToF spectra.

The spin echo length of CANISIUS was calibrated using a nanoporous alumina membrane from smartmembranes [44], similar to the method described in [45]. The pores used have a diameter of 40nm, with a pitch of 125nm and a thickness of 50 microns. For comparison the same sample was measured on the Larmor SESANS instrument at the ISIS pulsed neutron source. Since the spin echo length of Larmor is calibrated it is possible to extract the spin echo length of CANISIUS by matching the correlation functions measured using both instruments. Figure 7 shows the correlation function measured using CANISIUS superposed on measurements conducted with Larmor, in addition to an SEM image of the sample. The spin echo length axis of the CANISIUS measurement has been scaled to overlap with the Larmor measurement. Our measurement demonstrates the feasibility of the white beam SESANS measurement. Fitting a sphere model with a hardsphere structure factor to the data leads to a sphere diameter of 70 ± 10 nm. While differing significantly (3σ) from the actual pore diameter of 40 nm, the overlap between the white beam CANISIUS measurement and the Larmor measurement demonstrates the feasibility of the white beam method detailed in this work. The difference between the fitted diameter and the actual diameter may be explained by the fact that the nanopores are neither straight nor parallel. As a result when averaged over a large area the effective pore diameter is washed out.

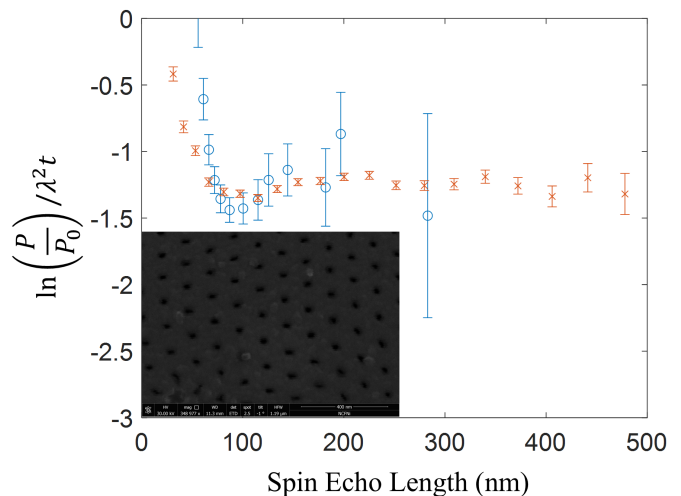


FIG. 7. Correlation functions measured using the white beam method on CANISIUS (blue) superposed on measurements conducted using Larmor (red). Both correlation functions are normalized by wavelength squared and sample thickness. The inset shows an SEM image of the nanoporous alumina, carried out by USTEM at the TU Wien.

Coherent Averaging

Constructing structured wavefunctions by coherent averaging is the main purpose of the CANISIUS instrument. This is done primarily to produce neutron wavefunctions that have non zero Orbital Angular Momentum (OAM) and investigate the properties of said states. We have demonstrated the method previously in perfect crystal neutron interferometry [10]. Here the structured wave

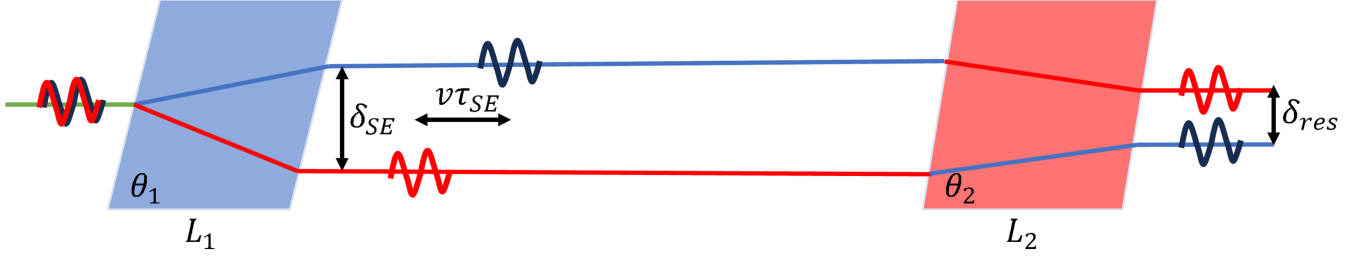


FIG. 8. Schematic representation of the coherent averaging mode of the CANISIUS instrument. This mode is almost equivalent to SESANS, the only difference being the different angles between the two field regions. This leads to an incomplete focusing of the two spin states, which is indicated by the residual distance δ_{res} between the states at the end of the instrument.

is produced by running the instrument in a SESANS like mode, where the first and second arm have different polshoe angles. As a result the two spin states retain some transverse separation after passing through the spin echo interferometer. The concept is illustrated in figure 8. This residual transverse separation is given by

$$\delta_{res} = \frac{\gamma m B L \lambda^2}{4\pi^2 \hbar} (\cot(\theta_1) - \cot(\theta_2)) \quad (14)$$

where we have assumed that $B = B_1 = B_2$ and $L = L_1 = L_2$. So for a Gaussian input wavefunction

$$\psi_0 = A e^{-x^2/\sigma^2} e^{ik_y y} \quad (15)$$

with σ the transverse coherence length the output wavefunction after spin selection would be equal to

$$\psi_1 = A' [e^{-(x - \frac{\delta_{res}}{2})^2/\sigma^2} + e^{i\eta} e^{-(x + \frac{\delta_{res}}{2})^2/\sigma^2}] e^{ik_y y} \quad (16)$$

with η a longitudinal phase between the two partial wavefunctions. η can be precisely tuned by changing the phase of one of the RF coils $\eta = 2\Delta\phi$. If δ_{res} is chosen appropriately with respect to the transverse coherence length σ and $\eta = \pi$, the wavefunction could be approximated by

$$\psi'_1 \propto \Pi\left(\frac{2k_x x}{\pi}\right) \sin(k_x x) e^{ik_y y} \quad (17)$$

such a wavefunction mimics a linearly polarized oscillation, which can also be described by two counter rotating oscillations. This can easily be shown by describing the above equation in cylindrical coordinates.

$$\psi'_1 \propto \frac{i}{2} \Pi\left(\frac{2k_x x}{\pi}\right) [e^{-ik_x r \cos \phi} - e^{ik_x r \cos(\phi)}] e^{ik_y y} \quad (18)$$

The exponential functions that have replaced the sine function can be expanded according to the Jacobi Anger expansion [46].

$$\psi'_1 \propto \frac{i}{2} \Pi\left(\frac{2k_x x}{\pi}\right) \left[\sum_{\ell} J_{\ell}(-k_x r) e^{i\ell\phi} - J_{\ell}(k_x r) e^{i\ell\phi} \right] e^{ik_y y} \quad (19)$$

Since Bessel functions are even for the zeroth mode and all even mode numbers ℓ this reduces to

$$\psi'_1 \propto -i \Pi\left(\frac{2k_x x}{\pi}\right) \sum_{\ell=\text{odd}} J_{\ell}(k_x r) e^{i\ell\phi} e^{ik_y y} \quad (20)$$

The rectangle function ensures that the ψ'_1 is only non zero for small arguments of the Bessel function. Since the Bessel function of order ℓ is proportional to z^{ℓ} (with z the argument), only the first order modes are relevant.

$$\psi'_1 \propto -i \Pi\left(\frac{2k_x x}{\pi}\right) \sum_{\ell=\pm 1} J_{\ell}(k_x r) e^{i\ell\phi} e^{ik_y y} \quad (21)$$

Similarly it can be shown that for a phase $\eta = 0$ the $\ell = 0$ and $\ell = \pm 2$ modes are generated. Even though the average OAM of each wavefunction produced by CANISIUS by coherent averaging is zero, the superpositions of $\ell = \pm 1$ or ± 2 are qualitatively different than the $\ell = 0$ mode, which are expected to scatter differently from nuclear targets [12, 13]. In addition the absorption characteristics of these states are expected to be different [14]. And as described in a recent paper these states may be used to explore the quantum Sagnac effect [47].

CONCLUSION

We have presented the new Austrian spin echo interferometer of the Atominstitut, CANISIUS and illustrated its capabilities, both as a ToF and a broad band white beam instrument. In particular we demonstrated the feasibility of polychromatic SESANS, which allows us to use the full potential of a continuous neutron source. This is especially important at weaker sources such as the 250 kW Triga reactor at the Atominstitut. Finally the coherent averaging capabilities of the instrument were illustrated. It was shown that CANISIUS is capable of producing neutrons that carry non zero OAM, in particular states that exist in a superposition of the $\ell = \pm 1$ modes. We expect this will be useful for exploring

OAM dependent scattering and absorption cross sections, in addition to exploring fundamental aspects of quantum mechanics from the quantum Sagnac effect to quantum information and contextuality.

ACKNOWLEDGMENTS

N. G. and S. S. acknowledge funding from the Austrian science fund (FWF), Project No. P34239, in addition N. G. is supported by the US Department of Energy (DOE) grant DE-SC0023695.

REFERENCES

-
- * niels.geerits@tuwien.ac.at
 † stephan.sponar@tuwien.ac.at
- [1] Yuji Hasegawa, Rudolf Loidl, Gerald Badurek, Matthias Baron, and Helmut Rauch. Violation of a bell-like inequality in single-neutron interferometry. *Nature*, 425:45–48, 2003.
 - [2] Y. Hasegawa, R. Loidl, G. Badurek, K. Durstberger-Rennhofer, S. Sponar, and H. Rauch. Engineering of triply entangled states in a single-neutron system. *Phys. Rev. A*, 81:032121, 2010.
 - [3] R. Colella, A. W. Overhauser, and S. A. Werner. Observation of gravitationally induced quantum interference. *Phys. Rev. Lett.*, 34:1472, 1975.
 - [4] M. G. Sagnac. The demonstration of the luminiferous aether by an interferometer in uniform rotation. *Comptes Rendus*, 157:708,1410, 1913.
 - [5] S. A. Werner, J. L. Staudenmann, and R. Colella. Effect of earth's rotation on the quantum mechanical phase of the neutron. *Phys. Rev. Lett.*, 42:1103–1106, 1979.
 - [6] Bahram Mashhoon. Neutron interferometry in a rotating frame of reference. *Physical Review Letters*, 61:2639–2642, 1988.
 - [7] Wenzel Kersten Hartmut Lemmel Richard Wagner Stephan Sponar and Yuji Hasegawa Armin Danner, Bülent Demirel. Spin-rotation coupling observed in neutron interferometry. *npj Quantum Information*, 6(23), 2020.
 - [8] R. Haun, F. E. Wietfeldt, M. Arif, M. G. Huber, T. C. Black, B. Heacock, D. A. Pushin, and C. B. Shahi. Precision measurement of the neutron scattering length of ^4He using neutron interferometry. *Phys. Rev. Lett.*, 124:012501, 2020.
 - [9] D. Sarenac, D. G. Cory, J. Nsofini, I. Hincks, P. Miguel, M. Arif, Charles W. Clark, M. G. Huber, and D. A. Pushin. Generation of a lattice of spin-orbit beams via coherent averaging. *PRL*, 121:183602, 2018.
 - [10] N. Geerits, H. Lemmel, A. Berger, and S. Sponar. Phase vortex lattices in neutron interferometry. *Nat. Comm. Phys.*, 6:209, 2023.
 - [11] D. Sarenac, C. Kapahi, W. Chen, C. W. Clark, D. G. Cory, M. G. Huber, I. Taminiau, K. Zhernenkov, and D. A. Pushin. Generation and detection of spin-orbit coupled neutron beams. *PNAS*, 116:20328–20332, 2019.
 - [12] A.V. Afanasev, D.V. Karlovets, and V.G. Serbo. Schwinger scattering of twisted neutrons by nuclei. *Phys. Rev. C*, 100:051601, 2019.
 - [13] A.V. Afanasev, D.V. Karlovets, and V.G. Serbo. Elastic scattering of twisted neutrons by nuclei. *Phys. Rev. C*, 103:054612, 2021.
 - [14] T. Jach and J. Vinson. Method for the definitive detection of orbital angular momentum states in neutrons by spin-polarized ^3He . *Phys. Rev. C*, 105:L061601, 2022.
 - [15] H. Rauch, W. Treimer, and U. Bonse. Test of a single crystal neutron interferometer. *Physics Letters A*, 47:369–371, 1974.
 - [16] Takuhiro Fujiie, Masahiro Hino, Takuya Hosobata, Go Ichikawa, Masaaki Kitaguchi, Kenji Mishima, Yoshichika Seki, Hirohiko M. Shimizu, and Yutaka Yamagata. Development of neutron interferometer using multilayer mirrors and measurements of neutron-nuclear scattering length with pulsed neutron source. *Phys. Rev. Lett.*, 132:023402, 2024.
 - [17] R. Gähler, R. Golub, K. Habicht, T. Keller, and J. Felber. Space-time description of neutron spin echo spectrometry. *Physica B: Condensed Matter*, 229:1–17, 1996.
 - [18] F. Mezei. Neutron spin echo: A new concept in polarized thermal neutron techniques. *Z. Physik*, 255:146–160, 1972.
 - [19] R. Golub and R. Gähler. A neutron resonance spin echo spectrometer for quasi-elastic and inelastic scattering. *Phys. Lett. A*, 123:43–48, 1987.
 - [20] R. Gähler, R. Golub, and T. Keller. Neutron resonance spin echo—a new tool for high resolution spectroscopy. *Physica B: Condensed Matter*, 180-181:899 – 902, 1992.
 - [21] S. Sponar, J. Klepp, C. Zeiner, G. Badurek, and Y. Hasegawa. Violation of a bell-like inequality for spin-energy entanglement in neutron polarimetry. *Phys. Lett. A*, 374:431–434, 2010.
 - [22] J. C. Leiner, S. J. Kuhn, S. McKay, J. K. Jochum, F. Li, A.A.M. Irfan, F. Funama, D. Mettus, L. Beddrich, C. Franz, J. Shen, S. R. Parnell, R. M. Dalgliesh, M. Loyd, N. Geerits, G. Ortiz, C. Pfeider, and R. Pynn. Spin-energy entanglement of a time-focused neutron. *Arxiv*, page 2404.07967v1, 2024.
 - [23] M.Theo Rekveldt. Novel sans instrument using neutron spin echo. *Nucl. Inst. and Meth. in Phys. Res. B*, 114:366–370, 1996.
 - [24] Victor-O. de Haan, Jeroen Plomp, Ad A. van Well, M. Theo Rekveldt, Yuji H. Hasegawa, Robert M. Dalgliesh, and Nina-Juliane Steinke. Measurement of gravitation-induced quantum interference for neutrons in a spin-echo spectrometer. *Phys. Rev. A*, 89:063611, 2014.
 - [25] S. R. Parnell, A. A. van Well, J. Plomp, R. M. Dalgliesh, N.-J. Steinke, J. F. K. Cooper, K. E. Steffen N. Geerits, W. M. Snow, and V. O. de Haan. Search for exotic spin-dependent couplings of the neutron with matter using spin-echo based neutron interferometry. *Phys. Rev. D*, 101:122002, 2020.
 - [26] J. Shen, S.J. Kuhn, R.M. Dalgliesh, V.O. de Haan, N. Geerits, A.A.M. Irfan, F. Li, S. Lu, S.R. Parnell, J. Plomp, A.A. van Well, A. Washington, D.V. Baxter, G. Ortiz, W.M. Snow, and R. Pynn. Unveiling contextual realities by microscopically entangling a neutron. *Nat. Commun.*, 11:930, 2020.

- [27] S. J. Kuhn, S. McKay, J. Shen, N. Geerits, R. M. Dalgliesh, E. Dees, A. A. M. Irfan, F. Li, S. Lu, V. Vangelista, D. V. Baxter, G. Ortiz, S. R. Parnell, W. M. Snow, and R. Pynn. Neutron-state entanglement with overlapping paths. *Phys. Rev. Research*, 3:023227, 2021.
- [28] R.M. Dalgliesh, S. Langridge, J. Plomp, V.O. de Haan, and A.A. van Well. Offspec, the isis spin-echo reflectometer. *Physica B: Condensed Matter*, 406:2346–2349, 2011.
- [29] N. Geerits, S. R. Parnell, M. A. Thijs, A. A. van Well, C. Franz, A. L. Washington, D. Raspon, R. M. Dalgliesh, and J. Plomp. Time of flight modulation of intensity by zero effort. *Review of Scientific Instruments*, 90:125101, 2019.
- [30] N. Geerits, S.R. Parnell, M.A. Thijs, W.G. Bouwman, and J. Plomp. Applying resonant spin flippers with poleshoes and longitudinal radio frequency fields to time of flight MIEZE. *Journal of Physics: Conference Series*, 1316:012011, 2019.
- [31] A.N. Bazhenov, V.M. Lobashev, A.N. Pirozhkov, and V.N. Slusar. *Nucl. Instr. and Meth. in Phys. Res. A*, 332:534–536, 1993.
- [32] Fankang Li, Steven R. Parnell, Hongyu Bai, Wencao Yang, William A. Hamilton, Brian B. Maranville, Rana Ashkar, David V. Baxter, J. Ted Cremer, and Roger Pynn. Spin echo modulated small-angle neutron scattering using superconducting magnetic wollaston prisms. *Journal of Applied Crystallography*, 49:55–63, 2016.
- [33] H. Rauch, J. Harms, and H. Moldaschl. A neutron spin-flip chopper for time-of-flight measurements, Sep 1968.
- [34] H. Freisleben and H. Rauch. Neutron spin-flip-chopper with high repetition rates. *Nuclear Instruments and Methods*, 98:61–67, 1972.
- [35] S. V. Grigoriev, R. Kreuger, W. H. Kraan, F. M. Mulder, and M. Th. Rekveldt. Neutron wave-interference experiments with adiabatic passage of neutron spin through resonant coils. *Phys. Rev. A*, 64:013614, 2001.
- [36] H. Rauch, H. Wolwitsch, H. Kaiser, R. Clothier, and S. A. Werner. Measurement and characterization of the three-dimensional coherence function in neutron interferometry. *Phys. Rev. A*, 53:902–908, 1996.
- [37] F. Li, R. Dadisman, and D. C. Wasilko. Optimization of a superconducting adiabatic radio frequency neutron resonant spin flipper. *Nuclear Inst. and Methods in Physics Research, A*, 955:163300, 2020.
- [38] Jeroen Plomp. *Spin-echo development for a time-of-flight neutron reflectometer*. Universal Press, 2009.
- [39] W. C. Chen, R. Erwin, P. Tsai, Md. T. Hassan, N. Hadad, and C. F. Majkrzak. A large beam high efficiency radio frequency neutron spin flipper. *Review of Scientific Instruments*, 92:063906, 2021.
- [40] E. Fermi, J. Marshall, and I. Marshall. A thermal neutron velocity selector and its application to the measurement of the cross section of boron. *Physical Review*, 72:193–196, 1947.
- [41] A.A. van Well and H. Fredrikze. On the resolution and intensity of a time-of-flight neutron reflectometer. *Physica B: Condensed Matter*, 357:204–207, 2005.
- [42] R. Pynn. Neutron spin-echo and three-axis spectrometers. *Journal of Physics E: Scientific Instruments*, 11:1133, 1978.
- [43] S. McKay, A. A. M. Irfan, Q. Le Thien, N. Geerits, S. R. Parnell, R. M. Dalgliesh, N. V. Lavrik, I. I. Kravchenko, G. Ortiz, and R. Pynn. Experimental evidence for the two-path description of neutron spin echo. *Phys. Rev. A*, 109:042420, 2024.
- [44] Smartmembranes, 2024. <http://www.smartmembranes.de/en/products/nanoporous-alumina/> [Accessed: 2024].
- [45] Fumiaki Funama, Caitlyn M. Wolf, Katie Weigandt, Jiazhou Shen, Steven R. Parnell, and Fankang Li. Spin echo small-angle neutron scattering using superconducting magnetic wollaston prisms. *Review of Scientific Instruments*, 95:073709, 2024.
- [46] M. Abramowitz and I. Stegun. *Handbook of Mathematical Functions with Formulas, Graphs, and Mathematical Tables*. Cambridge University Press, 1964.
- [47] N. Geerits, S. Sponar, K. E. Steffen, W. M. Snow, S. R. Parnell, G. Mauri, G. N. Smith, R. M. Dalgliesh, and V. de Haan. Measuring the angular momentum of a neutron using earth’s rotatio. *Arxiv*, page 2407.09307, 2024.